Available online at www.sciencedirect.com

jmr&t Journal of Materials Research and Technology

journal homepage: www.elsevier.com/locate/jmrt

Original Article

Ag and Zn doped TiO_2 nano-catalyst synthesis via a facile green route and their catalytic activity for the remediation of dyes

Faisal Ali [a], *Ghulam Moin-ud-Din* [a], *Munawar Iqbal* [b], *Arif Nazir* [a,*], *Imran Altaf* [c], *Norah Alwadai* [d,**], *Umme Habibah Siddiqua* [e], *Umer Younas* [a], *Abid Ali* [a], *Abida Kausar* [f], *Naveed Ahmad* [b]

[a] *Department of Chemistry, The University of Lahore, Lahore, Pakistan*
[b] *Department of Chemistry, Division of Science and Technology, University of Education, Lahore, Pakistan*
[c] *Institute of Microbiology, University of Veterinary and Animal Sciences, Lahore, Pakistan*
[d] *Department of Physics, College of Sciences, Princess Nourah bint Abdulrahman University, P.O. Box 84428, Riyadh, 11671, Saudi Arabia*
[e] *Department of Chemistry, University of Jhang, Jhang, Pakistan*
[f] *Department of Chemistry, Government College Women University Faisalabad, Pakistan*

ARTICLE INFO

Article history:
Received 4 November 2022
Accepted 2 February 2023
Available online 8 February 2023

Keywords:
Green synthesis
Nicotiana tabacum
Ag and Zn doping
Titanium dioxide
Catalytic activity
Textile dyes remediation

ABSTRACT

A facile green synthesis route was employed for the fabrication of Ag–Zn doped TiO_2 nano-catalyst and utilized for the remediation of dyes. *Nicotiana tabacum* leaves extract was used to prepare the Ag–Zn doped TiO_2 nano-catalyst by utilizing TiO_2 as precursor and $AgNO_3$, $ZnNO_3$ as doping agents. A strong UV–Vis spectra peak confirmed the Ag–Zn doped TiO_2 formation. Furior transformed infrared spectroscopy analysis revealed the role of phenolics in the *N. tabacum* leaves extract for the formation of Ag–Zn-doped TiO_2 nano-catalyst. Moreover, Ag–Zn doped TiO_2 nano-catalyst formation was confirmed by X-ray diffraction analysis, which reveals the cubic and tetragonal geometries with average size of 5.66 nm. The scanning electron microscopy analysis also confirmed the poly-morphological structure of prepared Ag–Zn doped TiO_2 nano-catalyst. The nano-catalyst was used for the remediation of dyes and conditions were optimized for maximum removal of dyes using $NaBH_4$ reducing agent. The catalytic activity results revealed that Ag–Zn doped TiO_2 showed promising features versus individual counterparts, which is correlated with reduced bandgap of doped nano-catalyst. The *N. tabacum* leaves extract efficiently stabilized Ag–Zn doped TiO_2 nano-catalyst that exhibited remarkable catalytic activity and have potential to treat the dyes in wastewater.

* Corresponding author.
** Corresponding author.
E-mail addresses: anmalik77@gmail.com (A. Nazir), nmalwadai@pnu.edu.sa (N. Alwadai).
https://doi.org/10.1016/j.jmrt.2023.02.011

1. Introduction

Dyes are a significant part of aquatic pollution released by the paper, tanning, cosmetic, textile and paint industries. Properties like structure uniqueness, chemical stability, different functional groups, and characteristic color of methyl orange and methylene blue make them relevant in industries [1–5]. Methyl orange is an azoic dye, and methylene blue is a thiazine dye. Wastewater containing these two compounds causes toxic effects on humans and aquatic life by getting into the food chain. The stability of dyes and their by-products makes them more hazardous due to their mutagenic and carcinogenic nature [6,7]. Due to their non-biodegradability conventional biological degradation methods are not applicable. Today scientists are extensively trying to remove or degrade these dyes from industrial waste before their release in freshwater bodies [8–11].

Physical and chemical methods like adsorption and degradation, respectively, are used to remove these dyes from wastewater. Photocatalytic degradation is a widely used method for degrading toxic dyes from water bodies with nanoparticles help. NPs are directly or indirectly involved in degrading more toxic dyes into less harmful by-products [12–14]. NPs TiO_2, Ag, Zn, Au, Pd, Cu, bi-metallic NPs Ag–Zn, Ag/Ni, Ag/Cu, Co/Fe, nano-composites like SnO_2 decorated polystyrene, carbon-doped TiO_2 and ZnO/CMC NCs are used for the catalytic degradation of dyes. Their activity in the visible region makes them photo-chemically active and efficient for dye degradation. Their small size and large surface area offer more active sites for the reaction to take place easily with less time compared to bulk material [9,15,16].

Metal and non-metal NPs have ostentatious catalytic properties compared to bulk materials. High surface-to-volume ratio, surface plasmon effect, catalytic, optical, conductivity, and thermal properties make their applications in wastewater treatment by catalytic and photocatalytic reduction of organic dyes. Bimetallic nanoparticles (BMNPs) show extraordinary results in almost all fields compared to monometallic or non-metallic NPs in technical and scientific fields. BMNPs alter the surface plasmon band, stability, and dispersion of NPs [17–19].

The number of metal-NPs comprising silver, zinc, TiO_2, gold, platinum, and cobalt have been synthesized through physical, chemical, biological, and green routes. NPs prepared by chemical methods cause pollution and have adsorbed harmful chemicals on their surface, causing annoying adversarial effects in the treatment and diagnostic fields. Physical methods are expensive. They follow a top-down technique and produce NPs having a narrow morphological range [20]. Biological route uses microorganisms, enzymes and fungus for the stabilization of NPs. Green synthesis is the best way to synthesize the metallic, bimetallic NPs due to no hazardous waste, low cost, ease of characterization and bottom-up technique make one able to control their morphology, crystallinity, and size [21,22].

This research work focusses on the use of *Nicotiana tabacum* (NT) dried leaves extract to synthesize Ag–Zn doped TiO_2 nano-catalysts (NCs). Identification techniques comprises UV VIS spectroscopy, FTIR, SEM and XRD were used for the confirmation, morphology, and crystallinity of prepared NCs. These prepared nano-catalysts were used for the catalytic and photocatalytic decolorization of methylene blue and methyl orange from industrial wastewater.

2. Material methods

2.1. Chemicals, instruments and reagents

Analytical grades reagents including $AgNO_3$ (≥99%), zinc nitrate hexahydrate $Zn(NO_3)_2.6H_2O$ (≥97%) were purchased from Fisher (UK) and TiO_2 (≥97%) was purchased from Sigma Aldrich (UK). All the reaction mixtures were prepared in deionized water. pH was optimized using NaOH. Fresh leaves of *N. tabacum* were collected from farms at Lodhraan Uggoki Sialkot, Pakistan.

2.2. Preparation of extract

Freshly collected leaves were cleaned with DI water 2–3 times to remove dust particles and dried in the oven at 40 °C. Fully dried leaves were crushed in fine powder using a grinder. 1 g of leaves powder in 200 mL of distilled water is heated on hotplate at 60 °C for 20 min greenish brown color solution is obtained which is filtered to separate leaves powder. The supernatant is stored in 4 °C for further use.

2.3. Synthesis of Ag–Zn doped TiO_2 NCs

Titanium oxide (TiO_2), silver nitrate ($AgNO_3$), and zinc nitrate hexa-hydrate ($ZnNO_3.6H_2O$) were used for starting precursors. In the synthesis of Ag–Zn doped TiO_2 NCs, 5 mM solution of TiO_2 with 5% (w/w) $AgNO_3$ and $ZnNO_3.6H_2O$ was dissolved in 100 mL of distilled water and stirred well as done previously [23]. This solution was added to leaves extract dropwise on continuous stirring at maintained pH, color changes occurred from greenish brown to white, which conformed the synthesis of NCs. The solution was further centrifuged and washed many time to remove the un-reacted ions.

2.4. Characterization of synthesized material

The NT stabilized Ag–Zn doped TiO_2 NCs were characterized by recording full scan of UV-VIS spectra from 300 to 800 nm and the surface plasmon of the NPs was also observed over UV-VIS Spectrophotometer CECIL CE 7400s Aquarius. Fourier transformation infrared spectroscopy (FTIR) by ATR was adopted to determine the functional groups using (Bruker, Alpha-II, UK) in the range of 4000–500 cm^{-1}. SEM morphologies were evaluated over (FE-SEM NOVA 450, UK). The crystalline nature was examined using an X-ray diffractometer (Bruker D-8 with Cu Kα $\Lambda = 1.54$ Å, UK).

2.5. Photocatalytic decolorization

Methylene blue (MB) and methyl orange (MO) were degraded photo catalytically using synthesized Ag–Zn doped TiO_2 NCs under direct sunlight. Decolorization of 0.01 mM MB and MO dyes has been studied by varying catalyst concentration

(1–5 mL of 0.2 mg/L) at maintained pH and 31 °C. The reaction mixtures were prepared and stirred under room light and then placed under sunlight for decolorization. Progress of the reaction was monitored by UV-VIS spectra ranging from 300 to 800 nm in specific time. Blue and orange color of dyes appeared in case of MB and MO, respectively [24–26].

2.6. Catalytic decolorization

MB and MO were degraded by using $NaBH_4$ reagent at prepared NCs catalyst and its factors were also studied to find the optimum concentrations of reagents for maximum decolorization. Dyes (MO, MB) and catalyst dose effects on decolorization were observed by varying concentration from 0.004 mM to 0.025 mM and 0.02 mg/mL to 0.1 mg/mL respectively in addition with 1.8 mM $NaBH_4$. The catalyst (Ag–Zn doped TiO_2) was confirmed over UV/Vis spectrophotometer at full scan of 300–800 nm. Absorbance peak of MB at 665 nm and that of MO at 460 nm was monitored for decolorization studies.

3. Results and discussion

In recent studies, synthesized Ag–Zn doped TiO_2 NCs using leaves extract without any external hazardous chemical stabilizing agent. In this study, obtained NCs were better in terms of size, which was improved than other reported methods [27]. Plant leaves extract itself acted for stabilization of doped NPs by controlling their size, prevented coalescence with controlled nucleation and ordered crystallinity of NPs. The methods which confirmed the formation of NCs are followed.

3.1. FTIR studies

FTIR analysis of NT stabilized Ag–Zn doped TiO_2 NCs was caries out to examine which biomolecules are responsible for their reduction and stabilization. Fig. 1 and Table 1 represents the transmittance peak at 3357, 2919, 2851, 1248, and 1091 cm^{-1}. The spectra of Ag–Zn doped TiO_2 NCs peak broad peak ranging from 3650 to 3100 indicating –OH stretching due to the water of crystallization adsorbed on the NCs [28], peaks located at 2919 and 2851 cm^{-1} exemplifies C–H stretching and peak at 1248 cm^{-1} illustrated amide (III) stretching of amino groups present in leaf extract. Peaks at 1593 cm^{-1} indicating C=C stretching [29]. Strong peak at 1091 cm^{-1} of C–O stretching [30]. Displacing of spectral lines from NT leave to NCs showed interconversion of functional groups for reduction and stabilization of NCs. Kumar et al. also reported the synthesis of silver NPs using NT leaf extract with peaks at 3403, 2934, 2396, 1761, 1624, 1384, 1075, cm^{-1} with almost similar functional groups [31].

Table 1 – Data of absorption peaks showing different functional groups using FTIR.

Sr. No.	Absorption Peaks	Functional Groups	References
1	3357 cm^{-1}	-OH stretching water molecules	[28]
2	2919 cm^{-1}	C–H Stretching	[32]
3	2851 cm^{-1}	C–H Stretching	[33]
4	1593 cm^{-1}	C=C Stretching	[29]
5	1248 cm^{-1}	Amide (III)	[34]
6	1091 cm^{-1}	C–O Stretching	[30]

3.2. XRD analysis

For the determination of crystalline nature of prepared Ag–Zn doped TiO_2 NCs XRD analysis performed under the range of 10–80°. Fig. 2 corresponds to XRD pattern peaks appeared at 2 θ having values 69.00°, 65.50°, 64.04°, 62.75°, 56.62°, 54.31°, 44.04°, 41.23°, 39.18°, 36.08° and 27.43° represent the TiO_2 (rutile) (JCPDS 75–1748), and additional peaks at 41.00°, 59.38° and 74.70° has confirmed the presence of AgZn (JCPDS 65–6585) as doped material. The presence of curve at lower angle may be due to its cubic structure and narrow peaks in the spectra are due to the nano-sized structure of the particles. High intensity peaks at 27.34° for 2 θ value is preferred orientation for synthesized nano-composites with comparatively lowest surface energy than other planes.

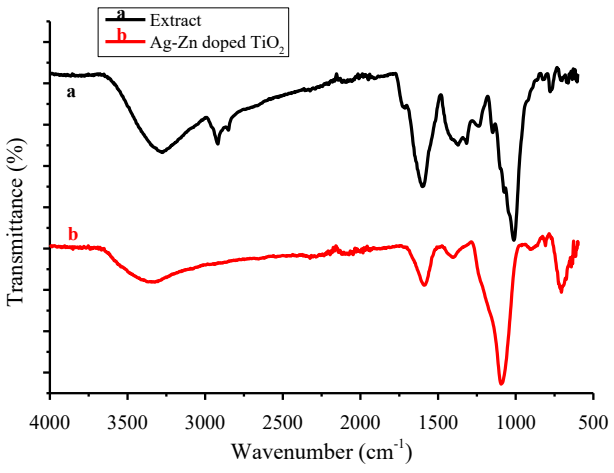

Fig. 1 – (A) FTIR of NT extract and (b) Ag–Zn doped TiO_2 NCs and plant extract showing different functionalities.

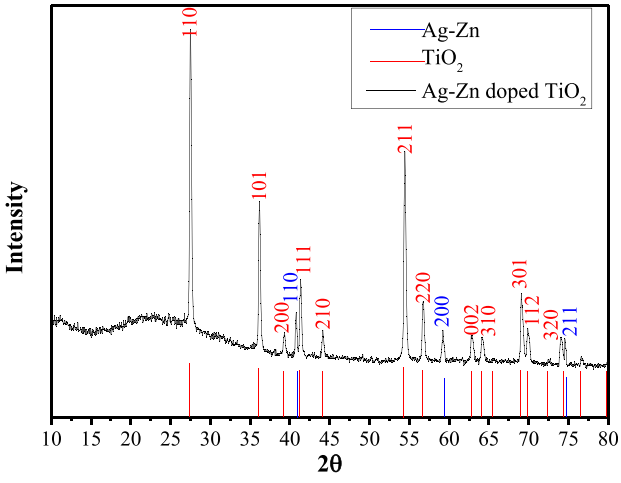

Fig. 2 – XRD Graph of Ag–Zn Doped TiO_2 NCs showing the crystalline nature of synthesized material.

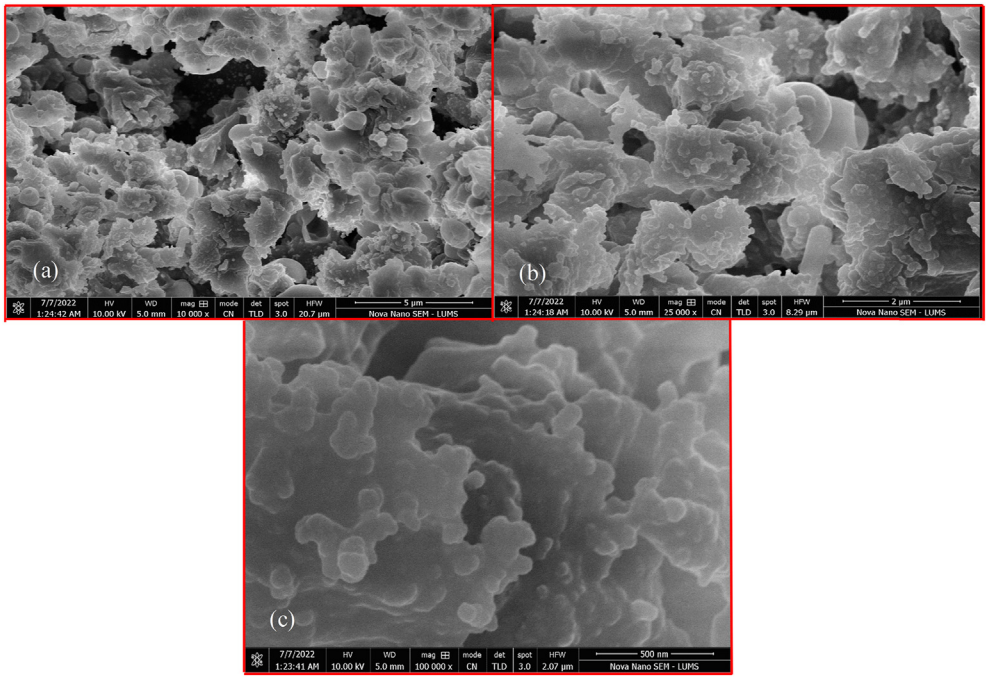

Fig. 3 – SEM Micrograph of (a–c) Ag–Zn doped TiO_2 NCs.

Debye Scherer equation applied for the determination of average size calculation of synthesized Ag–Zn doped TiO_2 NCs.

$$D_{avg} = \frac{k\lambda}{\beta \cos \theta}$$

Where k is dimensionless crystalline factor with value of 0.96, λ represents the wavelength of Ni–Cu Kα radiations and d and θ represents the full width half maximum in radian of each peak and angle is radiant, respectively. Average crystallite size of synthesized Ag–Zn doped TiO_2 NCs was found 5.66 nm.

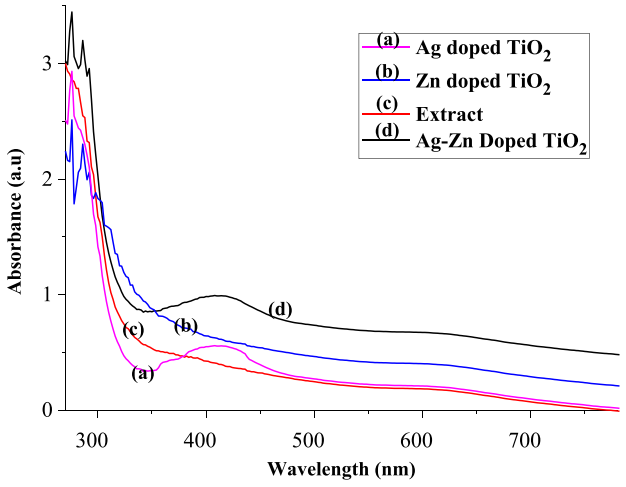

Fig. 4 – UV Vis spectra of (a) Ag doped TiO_2 (b) Zn doped TiO_2 (c) Plant extract and (d) Ag–Zn doped TiO_2 NCs, showing the wavelength of maximum absorption.

3.3. *Surface morphology*

Field emission scanning electron microscopy (FE-SEM) was utilized for the morphological and structural determination of fabricated Ag–Zn doped TiO_2 NCs (Fig. 3). It is defined that the NCs has a wide range morphology including clusters, rose petals like arrangements and nano-rods (Fig. 2a). NCs mainly formed and stabilized by the NT extract. As it is evident from the XRD analysis, the crystallite size of the Ag–Zn BMNPs was 5.66 nm. A variable shape (poly-morphological structure) was observed of Ag–Zn doped TiO_2 NCs. In earlier studies, it was shown that surface area and shape play a more significant impact in the adsorption and reduction of adsorbed molecules in catalytic processes. The wide range of morphology and large size of synthesized NCs was may be due to the doping of Ag–Zn BMNPs onto the surface of TiO_2 which is a well-known catalyst to enhanced the NCs catalytic properties by improving the energy bandgap and leads its vast range application in different fields [35].

3.4. *UV–vis analysis*

The UV-VIS spectroscopy was used to investigate the optical activity of Ag–Zn doped TiO_2 NCs. UV-VIS measurements verified the presence of co-doped NCs. Metallic NPs have some absorption maxima in the UV-VIS region; hence UV–vis spectrophotometric measurement can be used as a quick preliminary test to validate the nanoparticles fabrication. Sudden colour change was the primary sign of Ag–Zn doped TiO_2 NCs, Ag doped TiO_2 and Zn doped TiO_2 synthesis, and this change was then analyzed by UV–Vis spectrophotometer at wavelengths ranging 200–800 nm to find the surface plasmon resonance (SPR) of Ag NPs and lamda max of Zn NPs. Fig. 4 indicated a prominent peak at 400 nm in the UV–Vis

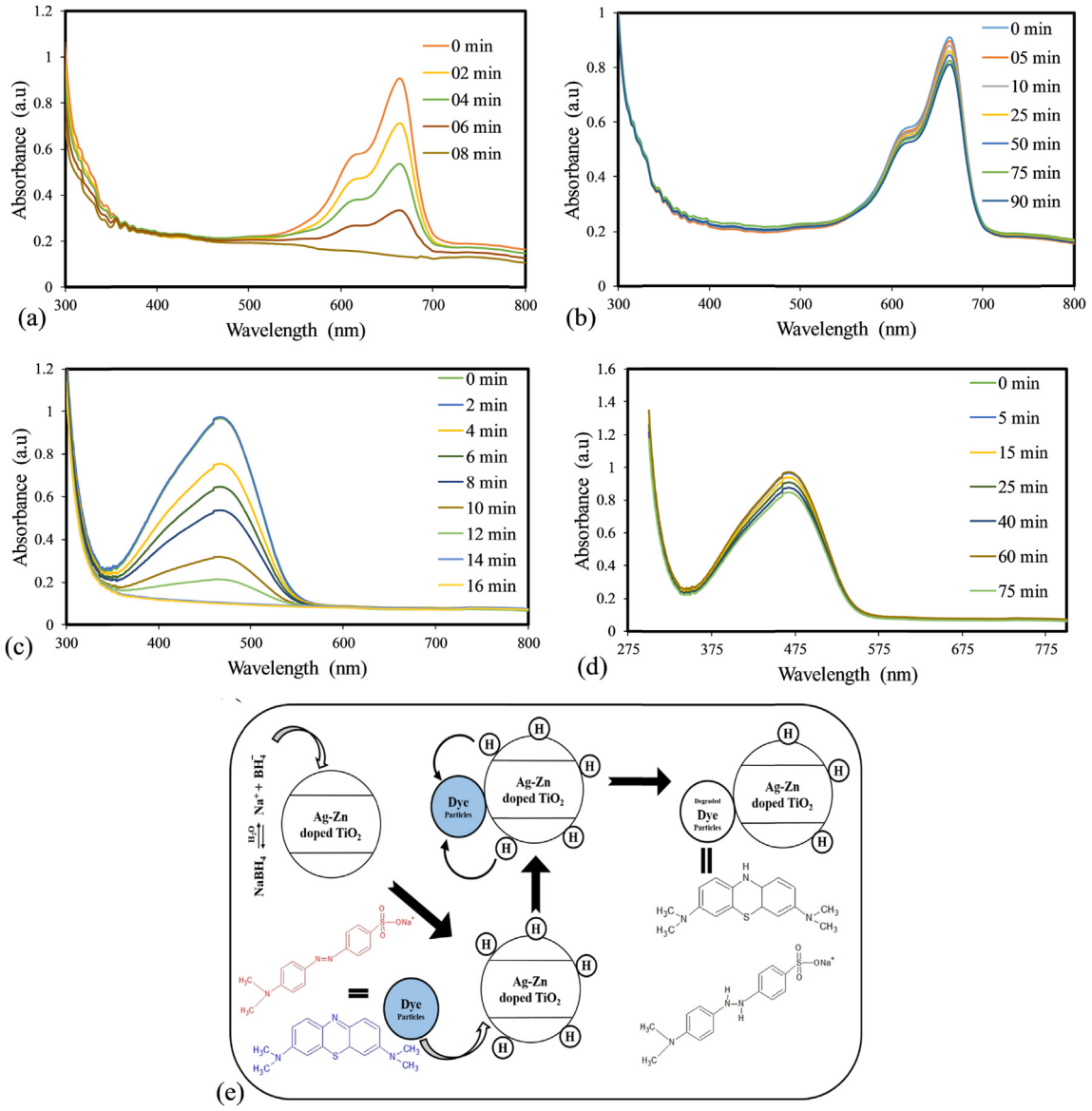

Fig. 5 – Catalytic decolorization of MB dye using (a) NCs and $NaBH_4$ at optimized conditions; 0.01 mM MB, 0.06 mg/mL catalyst, 1.8 mM $NaBH_4$ (b) without using catalyst; 0.01 mM MB, 1.8 mM $NaBH_4$ (c) MO catalytic decolorization using 0.01 mM MO, 1.8 mM $NaBH_4$, 0.1 mg/mL catalyst (d) without catalyst decolorization of MO dye using 0.01 mM MO, 1.8 mM $NaBH_4$ and (e) LH mechanism showing decolorization of MB dye.

spectra of greenly produced Ag doped TiO_2 and Ag–Zn doped TiO_2 NCs. Similarly, the previously results proven our results for peaks of TiO_2, ZnO and Ag NPs at 276 [36], 292 [37] and 420 nm [38] respectively. The minor displacement of the spectral peaks was observed for Ag doped TiO_2, Zn doped TiO_2 and Ag–Zn doped TiO_2 NCs, which was due to the doping and combined effect of bi-metals. These peaks were handful for the determination of bandgap.

3.5. *Catalytic studies*

Methylene blue (MB) is the widely used dye in major industries including cosmetics, fabrics, chemical, pharmaceutical, and agriculture industries. Almost 6 tons of dyes are wasted yearly in water which effect water bodies, animals and humans. These days, scientists are producing materials to reduce these dyes by adsorption, catalytic, photocatalytic decolorization and advanced oxidation processes. In our research we mainly focused to reduce MB catalytically, photo catalytically and different factors that affect the reduction of dyes including pH, Catalyst, dye and reducing agent concentrations [2,13,39]. Catalytic decolorization means reduction of dyes using a catalyst system which provide specific area for dye and reducing agent to adsorb and complete reaction of decolorization either by reduction or breakage of the compound. It is a slurry phase reaction in which catalyst is in solid phase and reactants are in liquid phase [17,40]. Herein, Ag–Zn doped TiO_2 NCs as the catalyst for the reduction and decolorization of MB dye has been done by using 0.01 mM MB, 1.8 mM $NaBH_4$ and 0.06 mg/mL catalyst concentrations as clearly shown in Fig. 5a.

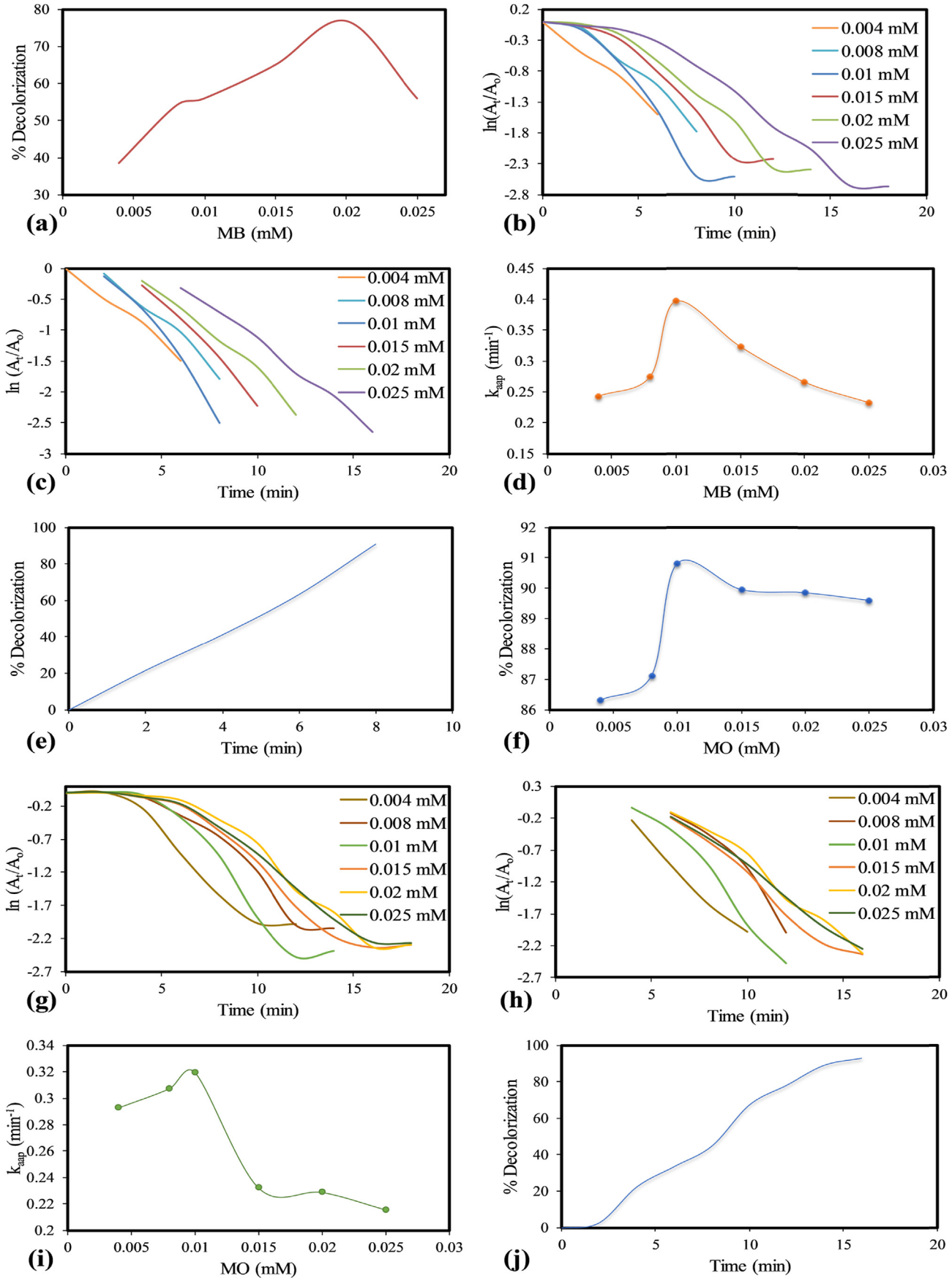

Fig. 6 – Effect of MB dye concentration on (a) % decolorization of MB dye using Ag–Zn doped TiO_2 NCs, (b) pseudo first order graph, (c) slopes obtained from pseudo first order reaction, (d) plot for k_{aap} vs. MB dye's concentration, (e) % decolorization of MB versus time (min), (f) effect of MO dye concentration on % decolorization of MO dye using Ag–Zn doped TiO_2 NCs, (g) MO dye decolorization's kinetic study, (h) its slopes, (i) rate constant of pseudo first for MO decolorization (j) % decolorization of MO dye vs. time (min).

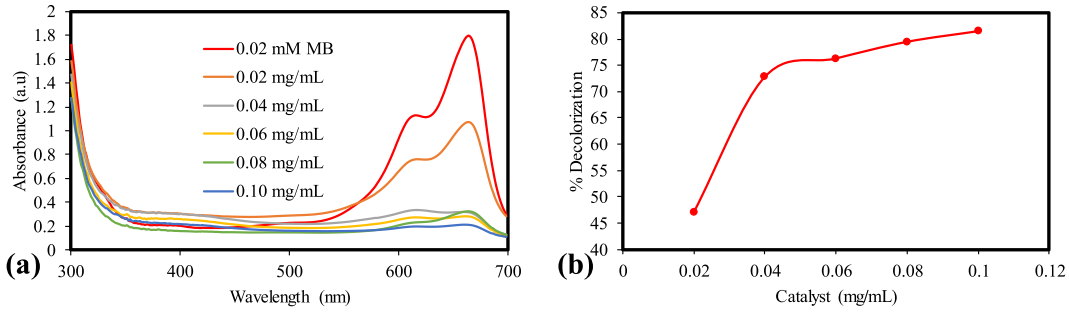

Fig. 7 – MB decolorization at (a) different TiO_2 doped Ag–Zn NCs' concentration and (b) decolorization (%) at 0.02–0.10 mg/mL NCs concentrations.

While, the decolorization also monitored in the absence of catalyst at same optimum conditions (Fig. 5b). The results revealed that after 90 min there was minimal effect of $NaBH_4$ for the decrease in the absorbance of MB dye. Similarly, MO dye decolorization was also studied at optimum conditions, 0.1 mM MO dye, 0.06 mg/mL catalyst and 1.8 mM $NaBH_4$ (Fig. 5c). The results were outstanding as the decolorization was completed in just 16 min and to confirm whether it is decolorization or just $NaBH_4$ is reducing the dye molecule, another reaction was done on same conditions but without catalyst presence (Fig. 5d). The results shown no decolorization after 75 min, which proven the efficacy of NCs catalyst. Decolorization of dye in the presence of reducing agent $NaBH_4$ and catalyst Ag–Zn doped TiO_2 has been explained on the basis of Langmuir Hinshelwood (LH) mechanism. Fig. 5e explains the decolorization mechanism of both dyes. First of all, reducing agent ionizes in water and produce BH^-_4 ions which get adsorb on the surface of catalyst and provide H^+ on it. At the same time, dye molecules get adsorb on the surface of catalyst and reaction starts in which double bonded nitrogen atom present in the dye molecule which give characteristic color and properties to dye molecules reduces by up taking of hydrogen from catalyst surface and reduction of dye occurred in almost 8 min. Different factors including effect of catalyst, effect of dye, effect of reducing agent, pH of solution and at various temperatures the rate of decolorization of dye has been studied. Previously decolorization of dye has been monitored using $NiFe_2O_4$ NPs [41].

3.5.1. *Effect of dyes initial concentration*

Decolorization of MB was studies under different initial dye concentrations range from 0.001 to 0.025 mM, 0.2 mg/L NT stabilized TiO_2 Ag–Zn doped TiO_2 NCs dose, 27 °C temperature and contact time of 8 min (Fig. 6a). MB colour removal was observed 73% at 0.020 mM concentration. After this concentration the decolorization decreases due the conjugation of dye molecules in solution. They face difficulty to reach at the surface of catalyst due to hyper conjugation and less molecules reach there to degrade [42]. It was previously reported that the decolorization of MB dye at Ag–Zn doped TiO_2 NCs was 25% in 8 min. So it can be stated that the decolorization of dye depends upon the initial concentration of dye. It would be maximum at 0.020 mM with 1 mL of 0.2 mg/L and decreases after and before this concentration.

Kinetic studies revealed the rate of the chemical reaction. Model reaction (Fig. 6b) explains that the decolorization of dye at 0.01 mM completed in just 8 min. The rate of the chemical reaction and different steps included in the complete decolorization of organic pollutant MB dye were studied (Fig. 6c). The reaction followed pseudo first order kinetics according to the equation

$$\ln(A_t / A_o) = -k_{app} \times t \quad (1)$$

It can be seen that at first there was very slow decolorization in 2 min which is induction time for the reaction to start, from 2 to 8 min' reaction speed up and completed in 8–10 min. The induction time, decolorization time and reaction completion time for different dye concentrations were different and almost increases with increase in concentration of dye. Fig. 6d and i explains the decolorization time of the catalytic reaction with same optimal conditions for MB and MO dyes' decolorization at which the rate of decolorization was comparatively very fast which was at 0.01 mM for both dyes [43]. The more time taken by the reaction to complete at higher dye concentration is due to the limited active sites at constant amount of catalyst in all the reaction mixtures. At higher concentration of dye, molecules of dye face difficulty of come and adsorb on the surface of catalyst due to steric hindrance and take more time for completion of reaction.

Decolorization of MB and MO with respected to time was observe and recorded in the form of percentage decolorization in Fig. 6e–j, which was 90% and 93% respectively. MO was completely degraded in just 16 min which is efficient as already reported decolorization time, which was about 90 to 60 min [44,45]. Kinetic studies revealed that the decolorization of MO dye was almost zero in first 5 min which could be called induction time. The next step was observed the decolorization time from 5 to 13 min and finally reaction completion time 13–16 min at different dye concentrations (Fig. 6g). Fig. 6h, corresponds to the slopes of pseudo first order catalytic decolorization kinetics of MO dye for the determination of k_{aap}. Further, Fig. 6i, shows the MO decolorization in terms of k_{aap}. This shows the remarkable effectiveness of NCs in the presence of $NaBH_4$ to degrade anionic dye (MO) as well as for cationic MB dye.

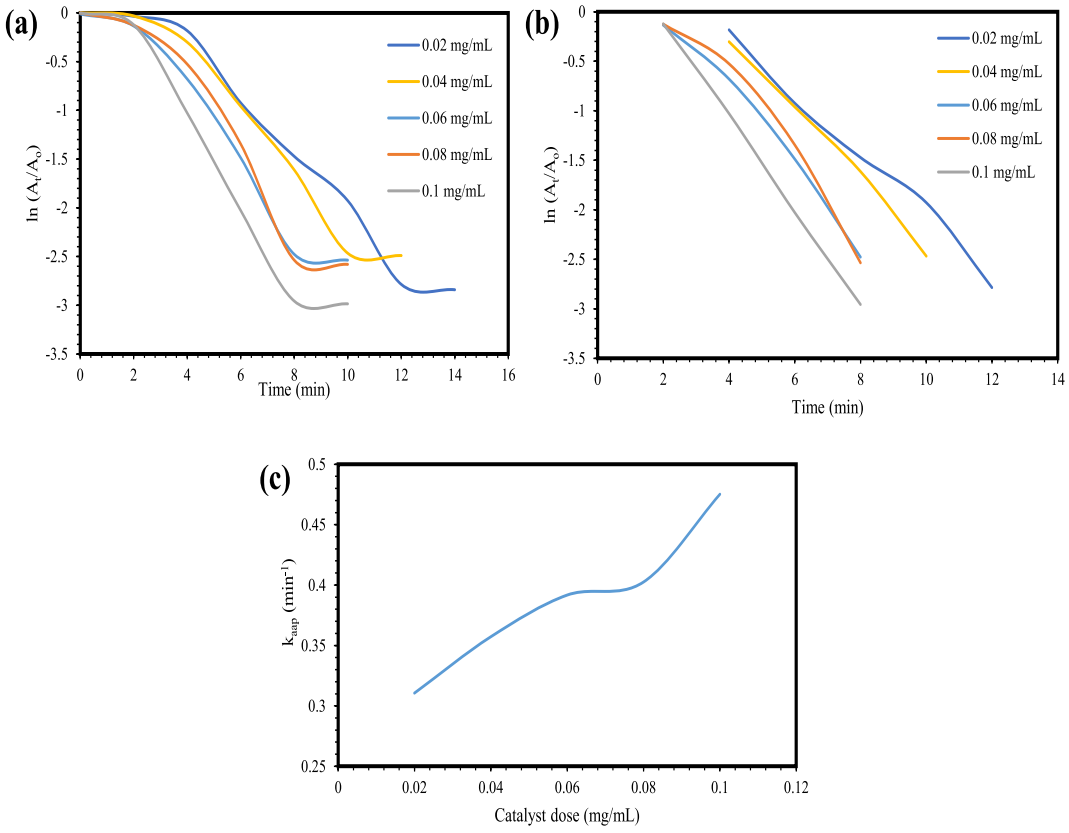

Fig. 8 – (A) Pseudo first order kinetics of MO decolorization (b) slopes of kinetics and (c) apparent rate constant vs time (min) of different catalyst concentrations.

3.5.2. *Catalyst dose effect*

To study that which concentration of catalyst is most suitable for maximum decolorization of methylene blue dye, different amount of catalyst ranging from 0.02 mg/mL to 0.10 mg/mL were used against 0.02 mM MB dye. Fig. 7a clearly shows that decolorization increases with increase in catalyst concentration. Fig. 7b shows the percentage decolorization of dye which more clearly explains that the decolorization of dye increases rapidly with increasing catalyst dose up to 1 mL and after this decolorization rate increases with very low rate. It means that 1 mL of catalyst dose if more reliable competitively for maximum decolorization of MB dye. By increasing the catalyst dose more active sites are available for catalytic decolorization but at very high concentration catalyst molecules hinders

Table 2 – Kinetics study for the decolorization of methylene blue dye.

Factors	MB (mM)	$NaBH_4$ (mM)	Ag–Zn doped TiO_2 NCs (mg/mL)	k_{app} (min^{-1})	Half-life ($t_{1/2}$) (min^{-1})	R^2
MB	0.004	1.8	0.06	0.2431	2.85068	0.9783
	0.008	1.8	0.06	0.2774	2.52551	0.9954
	0.01	1.8	0.06	0.3964	1.74823	0.9880
	0.015	1.8	0.06	0.3229	2.14618	0.9921
	0.02	1.8	0.06	0.2659	2.60624	0.9858
	0.025	1.8	0.06	0.2325	2.98065	0.9912
TiO_2 doped Ag–Zn	0.01	1.8	0.02	0.3106	2.23116	0.9840
MO	0.01	1.8	0.04	0.3572	1.94009	0.9540
	0.01	1.8	0.06	0.3917	1.76921	0.9997
	0.01	1.8	0.08	0.4025	1.72174	0.9954
	0.01	1.8	0.1	0.4751	1.45864	0.9899
	0.004	1.8	0.06	0.2928	2.36680	0.9891
	0.008	1.8	0.06	0.3074	2.25439	0.9427
	0.01	1.8	0.06	0.3195	2.16901	0.9767
	0.015	1.8	0.06	0.2322	2.98449	0.9798
	0.02	1.8	0.06	0.2289	3.02752	0.9861
	0.025	1.8	0.06	0.2157	3.21279	0.9961

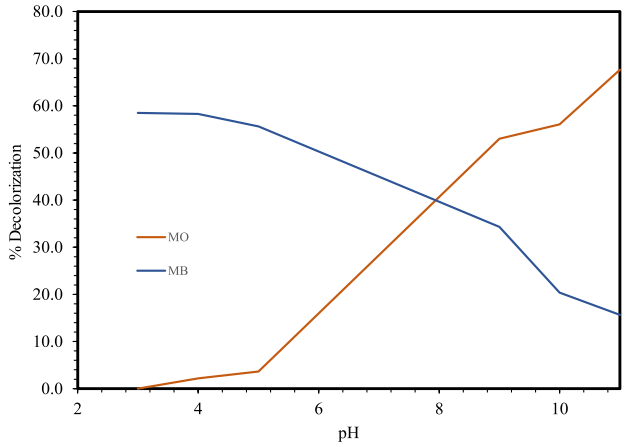

Fig. 9 – Effect of pH on decolorization (%) of MB and MO dye.

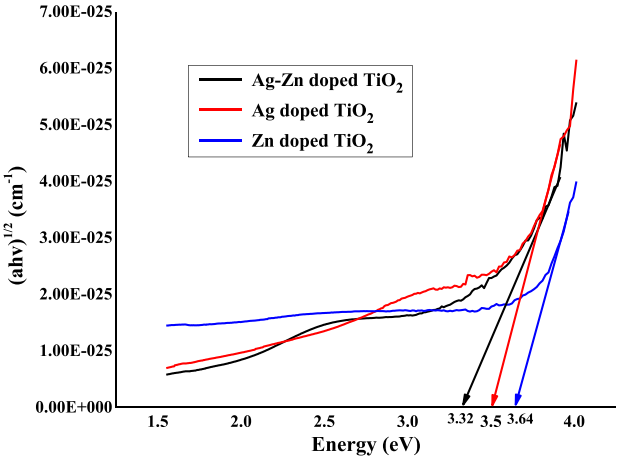

Fig. 11 – Energy bandgap of Ag–Zn doped TiO_2 NCs.

dye molecules to get adsorb on the specific active sites of the catalyst and react with the reducing agent to complete the reaction.

Kinetic of the reaction revealed the best concentration at which the rate of the reaction is maximum and give better results in decolorization of pollutants in water treatment. As shown in Fig. 8a, 0–2 min the reaction rate was almost zero at this state the molecules of the dye move towards the surface of Ag–Zn doped TiO_2 NCs, after this from 2 to 8 min the rate raised exponentially due to reaction between dye molecules and reducing agent, at the end the reaction completed in 8–10 min. Fig. 8b shows the negative slope for the determination of k_{app}. It can be seen clearly that the rate of the reaction was very fast for 0.1 mg/mL catalyst dose due to the availability of large number of active sites for the decolorization of dye. The rate increases with increase of catalyst dose which reveals that the rate of concentration varies directly with amount of catalyst shows the efficiency of the catalyst.

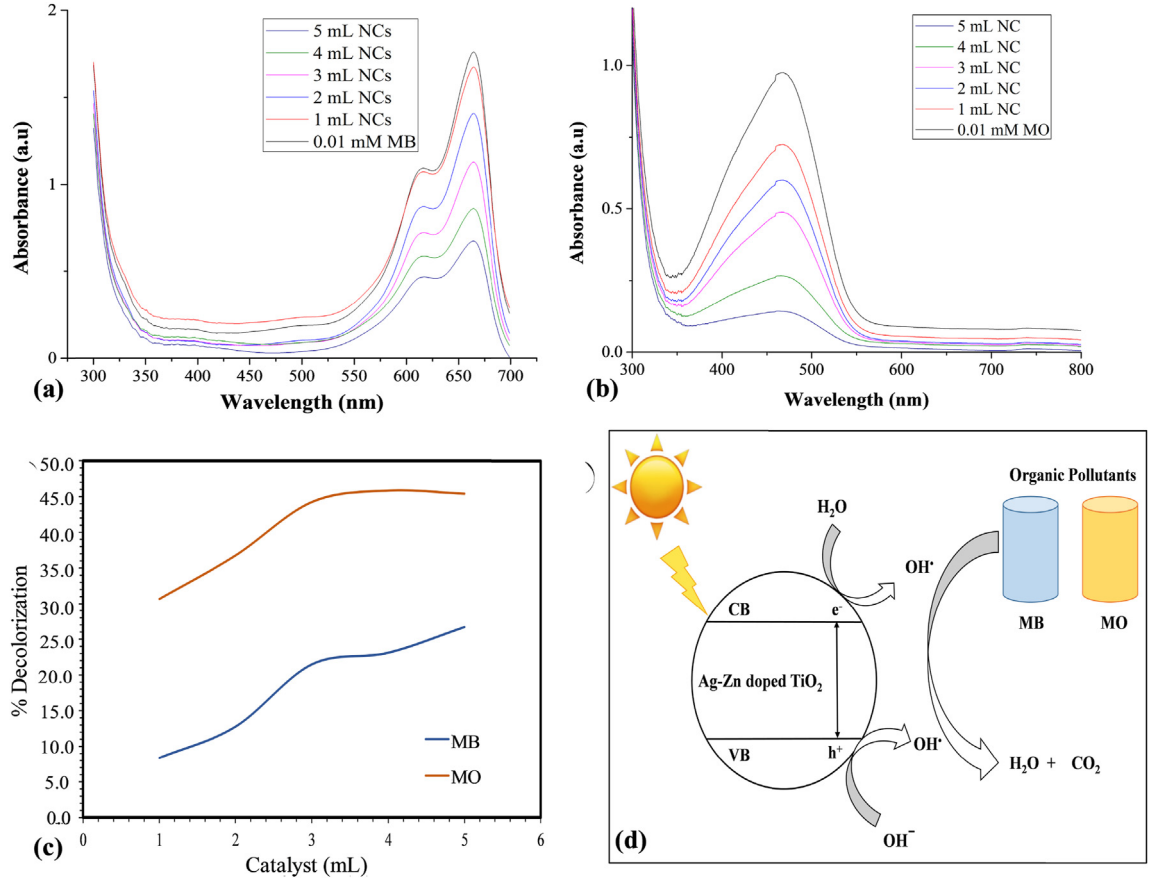

Fig. 10 – UV Vis spectra of photodecolorization of (a) MB, (b) MO at different catalyst dose; decolorization (%) of (c) 0.01 mM of MO and MB dyes at 1–5 mL of 2 mg/L NCs' concentrations and (d) photocatalytic decolorization mechanism.

Table 3 – Comparison of previously reported decolorization studies of different dyes and presnt study.

Nano-catalyst	Dye	Reducing agent	Decolorization (%)	Reaction time (min)	k_{aap}	References
Ag–Zn doped TiO_2 NC	MB	$NaBH_4$	90	8	0.2431	Current research
	MO		93	16	0.3195	
Au NPs	MB	$NaBH_4$	90.4	11.0	1.123	[51]
Ag-polystyrene-poly (Nisopropylmethacrylamide-acrylic acid)	Rh–B	$NaBH_4$	92	12	0.720	[52]
Ag –p (NMA)	CR	$NaBH_4$	87	16	0.047	[53]
PVA-PDA@Au beads	Rh–B	$NaBH_4$	90	60	–	[54]
zeolitic imidazolate framework-8 (ZIF-8)	Rh–B	$NaBH_4$	89	10	–	[55]
BiO–Br NWs	Rh–B	LIGHT	90.1	60	0.14966	[56]
Co NPs	CR	$NaBH_4$	83	23	0.047	[57]

Fig. 8c explains the k_{app} at different concentration of catalyst by keeping the concentration of dye and reducing agent constant. The value of half-life and observed rate constants are shown in Table 2 [46–48].

3.5.3. *Effect of pH*

Decolorization of dyes using nano-catalysts are greatly affected by pH of solution. The effect of pH on decolorization of methylene blue (MB) and methyl orange (MO) was studied by retaining its array from 3 to 11 at 0.01 mM and 0.0045 mM primary concentration of dyes respectively, 1 mL (0.2 mg/L) Ag–Zn doped TiO_2 NCs dose, 0.1% $NaBH_4$ at room temperature for 8 min and response is exposed in Fig. 9. Maximum MB removal was attained at highly acidic pH 3, it was 58.5% which gradually reduces to 15% at pH 11. Deceptively, the decolorization manner is acid-focused for MB. On other hand the removal of MO was maximum at highly basic pH 11, it was 67% and reduce to 0% at pH 3. Liu et al., 2017 reported that MB removal form waste water was higher at acidic medium and decreases with increase in pH of medium [49].

3.5.4. *Kinetic studies of decolorization*

Table 2 gives the complete description of apparent rate constant, regression factor and Half-life of the different concentrations of MB and Ag–Zn doped TiO_2 NCs dosage for decolorization of dye. It would be easy to select the optimum concentrations of reagents to get efficient decolorization of dye.

3.5.5. *Photo-catalytic studies*

The photocatalytic decolorization studies was observed on UV-VIS spectrophotometer with 300–800 nm range. The spectra were observed with initial 0.01 mM MB (Fig. 10a) and MO dye (Fig. 10b) concentration at 1–5 mL of 0.2 mg/L. The photo-catalytic decolorization of MB and MO was studied as the function of Ag–Zn doped TiO_2 NCs catalyst dose (Fig. 10c). Different conditions was adjusted including neutral pH and 180 min contact time at 26 °C room temperature. In case of MO the decolorization at 1 mL catalyst was 30% which increases to 45% at 5 mL catalyst dose after this decolorization remains constant this is due to the low absorption of light by the surface of catalyst to absorb and degrade the methyl orange. On other hand decolorization of MB increases with increase the catalyst dose. This is due to the increase the surface area for the MB molecules to be adsorbed by Ag–Zn doped TiO_2 NCs. In the presence of light, the surface of catalyst absorbs the light photon to excite electron from valence to conduction band and to generate hydroxyl ($OH^{\bullet}$) free radical to decolorize dye effectively (Fig. 10d).

3.5.6. *Energy bandgap*

The catalytic activity and photocatalytic activity of Ag–Zn Doped TiO_2 increased due to the reduced bandgap of TiO_2 after doping with Ag–Zn nano-particles. The bandgap of TiO_2 material was reported to be 3.4 eV [50]. The bandgaps for Ag, Zn and Ag–Zn doped TiO_2 was were calculated using UV-VIS studies (Fig. 4). In our studies the prepared nano-composites bear the bandgap of over 3 eV as shown in Fig. 11. This was the main reason for the efficient catalytic activity of Ag–Zn doped TiO_2 nano-composites. Table 3, illustrates some previously done work for decolorization of dyes.

4. Conclusions

Ag–Zn doped TiO_2 NCs were effectively synthesized utilizing 5% $AgNO_3$, $ZnCl_2$ on TiO_2 as a precursor and *Nicotiana Tabacum* leaves extract at 60 °C with continuous stirring. The *Nicotiana Tabacum* leaves extract acted as both a reducing and a stabilizing agent. The production of the Ag–Zn doped TiO_2 NCs was confirmed by UV–visible spectral peaks at 274, 296 and 400 nm. Ag–Zn doped TiO_2 NCs had an average crystallite size of 5.66 nm and a tetragonal geometry. The catalytic decolorization of MB-dye, $NaBH_4$, and Ag–Zn doped TiO_2NCs was then carried out using synthesized Ag–Zn doped TiO_2 NCs. Detailed analysis showed that the reaction was completed in 8 min, and kinetic analyses of the data supported the pseudo-first-order process having k_{app} value 0.2431 min^{-1}. Hence, *Nicotiana Tabacum* leaves extract can be used for synthesis of Ag–Zn doped TiO_2 NCs. The authors suggested that Ag–Zn doped TiO_2 NCs can be used to reduce azo-dyes, which can be a useful tool for treating wastwater from the textile industry.

Funding statement

This research was funded by Princess Nourah bint Abdulrahman University Researchers Supporting Project number (PNURSP2023R11), Princess Nourah bint Abdulrahman University, Riyadh, Saudi Arabia.

Declaration of Competing Interest

The authors declare that they have no known competing financial interests or personal relationships that could have appeared to influence the work reported in this paper.

Acknowledgments

The authors express their gratitude to Princess Nourah bint Abdulrahman University Researchers Supporting Project number (PNURSP2023R11), Princess Nourah bint Abdulrahman University, Riyadh, Saudi Arabia.

REFERENCES

[1] Noreen S, Khalid U, Ibrahim SM, Javed T, Ghani A, Naz S, et al. ZnO, MgO and FeO adsorption efficiencies for direct sky Blue dye: equilibrium, kinetics and thermodynamics studies. J Mater Res Technol 2020;9(3):5881–93.
[2] Mohsin M, Bhatti IA, Ashar A, Mahmood A, Maryam, Hassan Qu, et al. Fe/ZnO@ceramic fabrication for the enhanced photocatalytic performance under solar light irradiation for dye degradation. J Mater Res Technol 2020;9(3):4218–29.
[3] Arshad R, Bokhari TH, Javed T, Bhatti IA, Rasheed S, Iqbal M, et al. Degradation product distribution of Reactive Red-147 dye treated by UV/H2O2/TiO2 advanced oxidation process. J Mater Res Technol 2020;9(3):3168–78.
[4] Rahmat M, Rehman A, Rahmat S, Bhatti HN, Iqbal M, Khan WS, et al. Highly efficient removal of crystal violet dye from water by MnO2 based nanofibrous mesh/photocatalytic process. J Mater Res Technol 2019;8(6):5149–59.
[5] Bibi I, Nazar N, Ata S, Sultan M, Ali A, Abbas A, et al. Green synthesis of iron oxide nanoparticles using pomegranate seeds extract and photocatalytic activity evaluation for the degradation of textile dye. J Mater Res Technol 2019;8(6):6115–24.
[6] Sanda MDA, Badu M, Awudza JAM, Boadi NO. Development of TiO2-based dye-sensitized solar cells using natural dyes extracted from some plant-based materials. Chem Int 2021;7(1):9–20.
[7] Shindy H, El-Maghraby M, Goma M, Harb N. Heptamethine and nonamethine cyanine dyes: novel synthetic strategy, electronic transitions, solvatochromic and halochromic evaluation. Chem Int 2020;4(6):187–99.
[8] Sohail I, Bhatti IA, Ashar A, Sarim FM, Mohsin M, Naveed R, et al. Polyamidoamine (PAMAM) dendrimers synthesis, characterization and adsorptive removal of nickel ions from aqueous solution. J Mater Res Technol 2020;9(1):498–506.
[9] Naseer A, Ali A, Ali S, Mahmood A, Kusuma HS, Nazir A, et al. Biogenic and eco-benign synthesis of platinum nanoparticles (Pt NPs) using plants aqueous extracts and biological derivatives: environmental, biological and catalytic applications. J Mater Res Technol 2020;9(4):9093–107.
[10] Khan MI, Rasheed I, Naeem MA, Majeed S, Mustafa GM, Fatima M, et al. Structural, electrical and mechanical behavior evaluation of palladium doped diamond like carbon thin films. J Mater Res Technol 2020;9(4):8289–95.
[11] Bhatti HN, Hayat J, Iqbal M, Noreen S, Nawaz S. Biocomposite application for the phosphate ions removal in aqueous medium. J Mater Res Technol 2018;7(3):300–7.
[12] Siddiqua UH, Ali S, Hussain T, Iqbal M, Masood N, Nazir A. Application of multifunctional reactive dyes on the cotton fabric and conditions optimization by response surface methodology. J Nat Fibers 2022;19(3):1094–106.
[13] Khaliq N, Bibi I, Majid F, Arshad MI, Ghafoor A, Nazeer Z, et al. Mg1-xNixFe2-xCrxO4 synthesis via hydrothermal route: effect of doping on the structural, optical, electrical, magnetic and photocatalytic properties. Results Phys 2022;43:106059.
[14] Bokhari TH, Mustafa G, Ahmed N, Usman M, Akram N, Haq AU, et al. Degradation of a pigment red 238 using UV, UV/H_2O_2, UV/H_2O_2/SnO_2 and fenton processes. Pol J Environ Stud 2022;31(1):619–23.
[15] Shindy A. Problems and solutions in colors, dyes and pigments chemistry: a review. Chem Int 2017;3(2):97–105.
[16] Kamran U, Bhatti HN, Iqbal M, Nazir A. Green synthesis of metal nanoparticles and their applications in different fields: a review. Z Phys Chem 2019;233(9):1325–49.
[17] Nazir A, ur Rehman S, Abbas M, Iqbal DN, Ahsraf AR, Iqbal M. Green synthesis and characterization of copper nanoparticles using Parthenium hysterophorus extract: antibacterial and antioxidant activities evaluation. Chem Int 2022;8(2):68–76.
[18] Nazir A, Raza M, Abbas M, Abbas S, Ali A, Ali Z, et al. Microwave assisted green synthesis of ZnO nanoparticles using Rumex dentatus leaf extract: photocatalytic and antibacterial potential evaluation. Z Phys Chem 2022;236(9):1203–17.
[19] Ali F, Hamza M, Iqbal M, Basha B, Alwadai N, Nazir A. State-of-art of silver and gold nanoparticles synthesis routes, characterization and applications: a review. Z Phys Chem 2022;236(3):291–326.
[20] Ahmad B, Khan MI, Naeem MA, Alhodaib A, Fatima M, Amami M, et al. Green synthesis of NiO nanoparticles using Aloe vera gel extract and evaluation of antimicrobial activity. Mater Chem Phys 2022;288:126363.
[21] Ali F, Younas U, Nazir A, Hassan F, Iqbal M, Hamza B-u-z, et al. Biosynthesis and characterization of silver nanoparticles using strawberry seed extract and evaluation of their antibacterial and antioxidant activities. J Saudi Chem Soc 2022;26(6):101558.
[22] Nazir A, Akbar A, Baghdadi HB, ur Rehman S, Al-Abbad E, Fatima M, et al. Zinc oxide nanoparticles fabrication using Eriobotrya japonica leaves extract: photocatalytic performance and antibacterial activity evaluation. Arab J Chem 2021;14(8):103251.
[23] Ghazal S, Khandannasab N, Hosseini HA, Sabouri Z, Rangrazi A, Darroudi M. Green synthesis of copper-doped nickel oxide nanoparticles using okra plant extract for the evaluation of their cytotoxicity and photocatalytic properties. Ceram Int 2021;47(19):27165–76.
[24] Nazir A, Farooq S, Abbas M, Alabbad EA, Albalawi H, Alwadai N, et al. Synthesis, characterization and photocatalytic application of Sophora mollis leaf extract mediated silver nanoparticles. Z Phys Chem 2021;235(12):1589–607.
[25] Yasmin S, Nouren S, Bhatti HN, Iqbal DN, Iftikhar S, Majeed J, et al. Green synthesis, characterization and photocatalytic applications of silver nanoparticles using Diospyros lotus. Green Process Synth 2020;9(1):87–96.
[26] Jamil A, Bokhari TH, Javed T, Mustafa R, Sajid M, Noreen S, et al. Photocatalytic degradation of disperse dye Violet-26 using TiO2 and ZnO nanomaterials and process variable optimization. J Mater Res Technol 2020;9(1):1119–28.
[27] Kumar B, Smita K, Angulo Y, Cumbal L. Valorization of rambutan peel for the synthesis of silver-doped titanium dioxide (Ag/TiO2) nanoparticles. Green Process Synth 2016;5(4):371–7.
[28] Zafar MN, Dar Q, Nawaz F, Zafar MN, Iqbal M, Nazar MF. Effective adsorptive removal of azo dyes over

spherical ZnO nanoparticles. J Mater Res Technol 2019;8(1):713–25.
[29] Badawy AA, Abdelfattah NA, Salem SS, Awad MF, Fouda A. Efficacy assessment of biosynthesized copper oxide nanoparticles (CuO-NPs) on stored grain insects and their impacts on morphological and physiological traits of wheat (Triticum aestivum L.) plant. Biology 2021;10(3):233.
[30] Asghar MA, Zahir E, Asghar MA, Iqbal J, Rehman AA. Facile, one-pot biosynthesis and characterization of iron, copper and silver nanoparticles using Syzygium cumini leaf extract: as an effective antimicrobial and aflatoxin B1 adsorption agents. PLoS One 2020;15(7):e0234964.
[31] Kumar SP, Darshit P, Ankita P, Palak D, Ram P, Pradip P, et al. Biogenic synthesis of silver nanoparticles using Nicotiana tobaccum leaf extract and study of their antibacterial effect. Afr J Biotechnol 2011;10(41):8122–30.
[32] Daphedar A, Taranath TC. Characterization and cytotoxic effect of biogenic silver nanoparticles on mitotic chromosomes of Drimia polyantha (Blatt. & McCann) Stearn. Toxicol Rep 2018;5:910–8.
[33] Sangeetha MK, Mariappan M, Madhurambal G, Mojumdar SC. Synthesis growth and characterization of l-valine nickel (II) chloride. J Therm Anal Calorim 2012;108(3):887–94.
[34] Khyade MS, Varpe SN, Padwal AD. Evaluation of chemical profile and antioxidant potential of Trichodesma indicum (L.) R.Br. Int J Phytomed 2017;9(3):416.
[35] Karimi-Shamsabadi M, Behpour M. Comparing photocatalytic activity consisting of Sb2S3 and Ag2S on the TiO2–SiO2/TiO2 nanotube arrays-support for improved visible-light-induced photocatalytic degradation of a binary mixture of basic blue 41 and basic red 46 dyes. Int J Hydrogen Energy 2021;46(53):26989–7013.
[36] Rajakumar G, Rahuman AA, Roopan SM, Chung I-M, Anbarasan K, Karthikeyan V. Efficacy of larvicidal activity of green synthesized titanium dioxide nanoparticles using Mangifera indica extract against blood-feeding parasites. Parasitol Res 2015;114(2):571–81.
[37] El-Belely EF, Farag MM, Said HA, Amin AS, Azab E, Gobouri AA, et al. Green synthesis of zinc oxide nanoparticles (ZnO-NPs) using Arthrospira platensis (Class: cyanophyceae) and evaluation of their biomedical activities. Nanomaterials 2021;11(1):95.
[38] Eid AM, Fouda A, Niedbała G, Hassan SE-D, Salem SS, Abdo AM, et al. Endophytic Streptomyces laurentii mediated green synthesis of Ag-NPs with antibacterial and anticancer properties for developing functional textile fabric properties. Antibiotics 2020;9(10):641.
[39] Khan MI, Hasan MS, Bhatti KA, Rizvi H, Wahab A, Rehman S-u, et al. Effect of Ni doping on the structural, optical and photocatalytic activity of MoS2, prepared by Hydrothermal method. Mater Res Express 2020;7(1):015061.
[40] Shammout MW, Awwad AM. A novel route for the synthesis of copper oxide nanoparticles using Bougainvillea plant flowers extract and antifungal activity evaluation. Chem Int 2021;7(1):71–8.
[41] Atacan K, Güy N, Çakar S, Özacar M. Efficiency of glucose oxidase immobilized on tannin modified NiFe2O4 nanoparticles on decolorization of dye in the Fenton and photo-biocatalytic processes. J Photochem Photobiol Chem 2019;382:111935.
[42] Nwamezie OUIF. Green synthesis of iron nanoparticles using flower extract of Piliostigma thonningii and their antibacterial activity evaluation. Chem Int 2018;4(1):60–6.
[43] Ali F, Ali Z, Younas U, Ahmad A, Mooin-ud-din G, Pervaiz M, et al. UV-light mediated biosynthesis of silver nanowires; characterization, dye degradation potential and kinetic studies. Sustainability 2021;13(23):13220.
[44] Tantawy HR, Nada AA, Baraka A, Elsayed MA. Novel synthesis of bimetallic Ag-Cu nanocatalysts for rapid oxidative and reductive degradation of anionic and cationic dyes. Applied Surface Science Advances 2021;3:100056.
[45] Shah BR, Patel UD. Aqueous pollutants in water bodies can be photocatalytically reduced by TiO2 nano-particles in the presence of natural organic matters. Separ Purif Technol 2019;209:748–55.
[46] Nazir A, Zahid S, Mahmood Z, Kanwal F, Latif S, Imran M, et al. Adsorption kinetics for the removal of toxic Congo red dye by polyaniline and citrus leaves as effective adsorbents. Z Phys Chem 2022;236(10):1301–19.
[47] Khera RA, Iqbal M, Ahmad A, Hassan SM, Nazir A, Kausar A, et al. Kinetics and equilibrium studies of copper, zinc, and nickel ions adsorptive removal on to Archontophoenix alexandrae: conditions optimization by RSM. Desalination Water Treat 2020;201:289–300.
[48] Mukhtar A, Ghulam A, Rizwan H, Fatima J, Ghulam Abbas S, Gul Afshan S, et al. Kinetics and equilibrium studies of eriobotrya japonica: a novel adsorbent preparation for dyes sequestration. Z Phys Chem 2019;233(10):1469–84.
[49] Liu Y, Jin W, Zhao Y, Zhang G, Zhang W. Enhanced catalytic degradation of methylene blue by α-Fe2O3/graphene oxide via heterogeneous photo-Fenton reactions. Appl Catal B Environ 2017;206:642–52.
[50] Kripal R, Vaish G, Tripathi UM. Comparative study of EPR and optical properties of CdS, TiO2 and CdS-TiO2 nanocomposite. J Electron Mater 2019;48(3):1545–52.
[51] Miah AT, Bharadwaj SK, Saikia P. Surfactant free synthesis of gold nanoparticles within meso-channels of non-functionalized SBA-15 for its promising catalytic activity. Powder Technol 2017;315:147–56.
[52] Naseem K, Begum R, Wu W, Irfan A, Al-Sehemi AG, Farooqi ZH. Catalytic reduction of toxic dyes in the presence of silver nanoparticles impregnated core-shell composite microgels. J Clean Prod 2019;211:855–64.
[53] Iqbal S, Zahoor C, Musaddiq S, Hussain M, Begum R, Irfan A, et al. Silver nanoparticles stabilized in polymer hydrogels for catalytic degradation of azo dyes. Ecotoxicol Environ Saf 2020;202:110924.
[54] Li Y, Lu H, Wang Y, Li X. Deposition of Au nanoparticles on PDA-functionalized PVA beads as a recyclable catalyst for degradation of organic pollutants with NaBH4 in aqueous solution. J Alloys Compd 2019;793:115–26.
[55] Chirra S, Wang L-F, Aggarwal H, Tsai M-F, Soorian SS, Siliveri S, et al. Rapid synthesis of a novel nano-crystalline mesoporous faujasite type metal-organic framework, ZIF-8 catalyst, its detailed characterization, and NaBH4 assisted, enhanced catalytic Rhodamine B degradation. Mater Today Commun 2021;26:101993.
[56] Yan Y, Yang H, Yi Z, Wang X, Li R, Xian T. Evolution of Bi nanowires from BiOBr nanoplates through a NaBH4 reduction method with enhanced photodegradation performance. Environ Eng Sci 2020;37(1):64–77.
[57] Khan MN, Bashir O, Khan TA, Al-Thabaiti SA, Khan Z. Catalytic activity of cobalt nanoparticles for dye and 4-nitro phenol degradation: a kinetic and mechanistic study. Int J Chem Kinet 2017;49(6):438–54.